THE JOURNAL OF PHYSICAL CHEMISTRY B

ARTICLE

pubs.acs.org/JPCB

A Refined MS-EVB Model for Proton Transport in Aqueous Environments

Kyoyeon Park,[†] Wei Lin,[†] and Francesco Paesani*

Department of Chemistry and Biochemistry, University of California, San Diego, 9500 Gilman Drive, La Jolla, California 92093, United States

ABSTRACT: In order to improve the description of proton mobility in aqueous environments, a revised multistate empirical valence bond model (*a*MS-EVB3) is developed. The new *a*MS-EVB3 model is built upon an anharmonic water force field (*a*SPC/Fw) in which the OH bond potential is described through a quartic approximation to a Morse potential. First, it is shown that the *a*SPC/Fw anharmonic water model provides an accurate description of water at ambient conditions and reproduces the available experimental data for several structural, thermodynamic, and dynamical properties. Second, it is shown that, when applied to the study of proton solvation and transport in bulk water, the new *a*MS-EVB3 model accurately describes the solvation structure around the excess proton. Importantly, the new *a*MS-EVB3 model predicts a significantly larger proton diffusion coefficient than previous models, which largely improves the agreement with the available experimental data.

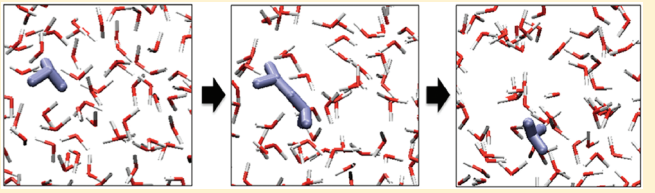

1. INTRODUCTION

Since water plays a central role in many fundamental phenomena (e.g., reactive, transport and diffusion processes in solution and at interfaces, and hydration of biomolecules), it is not surprising that much experimental and theoretical effort has been devoted in the past to the development of a molecular-level understanding of its unique properties.[1,2] On the other hand, proton solvation and transport processes take place in a variety of chemical reactions in solution that have important implications in many different areas including atmospheric chemistry, energy transduction, and the development of proton exchange membrane fuel cells, just to mention a few.[3,4] It is thus apparent that an accurate modeling of the structural, thermodynamic, and dynamical properties of pure and protonated water plays a key role for a complete understanding of the molecular mechanisms that govern several important physicochemical processes in the condensed phase.

From a computational standpoint, numerous water force fields have been developed, which include minimalistic models based on coarse-grained representations of the molecular interactions,[5,6] atomistic models based on fixed partial charges and rigid bonds,[7−10] and more sophisticated models that explicitly take into account for molecular flexibility,[11] three-body contributions,[12−14] and electronic polarization.[15−17] Specialized models have also been developed to account for nuclear quantum effects.[18−20] When employed in computer simulations, each of these models has shown a certain degree of success in reproducing at least some of the properties of liquid water. In this regard, since water often represents the most abundant component in fully atomistic computer simulations of condensed phase systems (e.g., biomolecules in solution), the largest fraction of CPU time used to model these systems is effectively spent in the calculation of the interactions between water molecules. As a consequence, it is highly desirable to have access to water models that can accurately describe the structural, thermodynamic, and dynamical properties of the liquid phase and, at the same time, can still be computationally affordable. These requirements become even more critical for molecular simulations of the behavior of excess protons in aqueous environments. Because of the high mobility of protons in water, realistic computer models must be capable of describing the hopping dynamics of protons between water molecules within the hydrogen-bond network. This implies that both the Grotthuss mechanism[21] and the associated delocalization of the excess charge over multiple water molecules[22] have to be correctly taken into account. Although both these features can in principle be captured in ab initio molecular dynamics (AIMD) simulations, current approaches based on density functional theory (DFT) have been limited so far to relatively small systems due to the associated high computational cost.[4] It should also be noted that the choice of the most appropriate functional for describing the water properties is still a matter of debate, with recent studies highlighting the importance of the dispersion interactions, which instead are usually neglected in the most common DFT implementations.[23−26]

Alternatively, reactive force fields can also be used to describe the physicochemical properties of protons in aqueous environments. Among the most effective approaches based on a force field representation of the molecular interactions is the multistate empirical valence bond (MS-EVB) method.[27−33] Built upon the original empirical valence bond (EVB) method introduced by

Received: September 16, 2011
Revised: November 12, 2011
Published: November 22, 2011

Warshel for a fixed number of empirically determined valence bond states,[34] the MS-EVB method enables the description of proton solvation and transport by evolving the system on a reactive potential energy surface defined by a linear combination of multiple diabatic potentials that are dynamically selected during the simulation. Each diabatic state corresponds to a limiting "state" of the system, with the total number of all possible states representing an effective basis set for the system Hamiltonian. By construction, the MS-EVB method captures the main features of the Grotthuss mechanism in which the proton hopping events are strictly connected to both the molecular diffusion and the rearrangement of the water hydrogen-bond network.[3,4] Since its initial development, the MS-EVB method has been applied with success to study proton solvation and transport in many different environments and under different conditions (see ref 3 for a recent review). Recently, the latest version of the MS-EVB model, MS-EVB3, has also been employed to elucidate the elementary steps associated with proton transfer in bulk water.[35] Despite much success in reproducing the essential features and molecular mechanisms of proton transport and solvation in aqueous environments, all previous MS-EVB models have been found to underestimate the diffusion coefficient associated with the proton mobility in bulk water. The only exception is represented by a polarizable version of the MS-EVB approach.[36]

In order to provide a more quantitative description of proton transport in aqueous environments, a refined version of the (nonpolarizable) MS-EVB3 model is developed in this work. The new model is based on an anharmonic water force field in which the OH intramolecular vibrations are represented by a quartic approximation to the Morse potential. This functional form has been shown to provide a reasonable representation of the OH stretching frequencies in pure water when nuclear quantum effects are explicitly taken into account.[20,37] The introduction of vibrational anharmonicity into the original SPC/Fw water force field,[11] which is employed in the MS-EVB3 model,[30,31] leads to a new anharmonic water model, *a*SPC/Fw. The latter clearly satisfies the requirement to be simple and fast to calculate using standard algorithms for molecular simulations and, importantly, provides a more realistic description of the water motion. In turn, the explicit account of the vibrational anharmonicity in the description of the water interactions also leads to a refined anharmonic MS-EVB3 model, *a*MS-EVB3. When applied to the study of proton solvation and transport in bulk water, the new *a*MS-EVB3 predicts a proton diffusion coefficient that is significantly larger (~40%) than the value calculated with the original MS-EVB3 model and, consequently, in better agreement with the available experimental data. However, some differences still exist between the experimental and MS-EVB results, which may be due to several factors that are discussed in this study. The paper is organized as follows: in section 2, the computational methodologies are described, while the results are illustrated in section 3. The conclusions are then given in section 4.

2. COMPUTATIONAL METHODOLOGIES

2.1. Anharmonic *a*SPC/Fw Water Model. Taking as a reference the original (harmonic) SPC/Fw water model,[11] an anharmonic force field (*a*SPC/Fw) was developed in order to accurately reproduce several structural, thermodynamic, and dynamical properties of bulk water at room temperature (T = 298.15 K). The functional form of the *a*SPC/Fw force field

Table 1. Parameters for the *a*SPC/Fw Model

r_{OH}^{eq} (Å)	0.995
D_{OH} (kcal mol^{-1})	116.09
α_{OH} (Å^{-1})	2.287
K_{HOH} (kcal mol^{-1} rad^{-2})	75.9
θ_{HOH}^{eq} (deg)	112.5
q_O (e)	−0.8350
q_H (e)	0.4175
ε_{OO} (kcal mol^{-1})	0.1554253
σ_{OO} (Å)	3.165492

is expressed as

$$V = V^{bond} + V^{angle} + V^{inter} \quad (1)$$

where

$$V^{bond} = D_{OH}\left[\alpha_{OH}^2(r_{OH_1}\text{-}r_{OH}^{eq})^2 - \alpha_{OH}^3(r_{OH_1}\text{-}r_{OH}^{eq})^3 + \frac{7}{12}\alpha_{OH}^4(r_{OH_1}\text{-}r_{OH}^{eq})^4\right] + D_{OH}\left[\alpha_{OH}^2(r_{OH_2} - r_{OH}^{eq})^2 - \alpha_{OH}^3(r_{OH_2} - r_{OH}^{eq})^3 + \frac{7}{12}\alpha_{OH}^4(r_{OH_2}\text{-}r_{OH}^{eq})^4\right] \quad (2)$$

$$V^{angle} = \frac{K_{HOH}}{2}(\theta_{HOH} - \theta_{HOH}^{eq})^2 \quad (3)$$

and

$$V^{inter} = \sum_{i,j}\left\{4\varepsilon_{ij}\left[\left(\frac{\sigma_{ij}}{R_{ij}}\right)^{12} - \left(\frac{\sigma_{ij}}{R_{ij}}\right)^{6}\right] + \frac{q_i q_j}{R_{ij}}\right\} \quad (4)$$

In eqs 1−4, V^{bond} represents the anharmonic OH stretching potential, V^{angle} describes the HOH bending potential, and V^{inter} describes the intermolecular interactions that include both the Lennard-Jones and Coulomb terms between all pairs of nonbonded atoms. In eqs 2 and 3, r_{OH}^{eq} and θ_{HOH}^{eq} are the equilibrium bond length and angle of an isolated water molecule, respectively, while R_{ij} in eq 4 is the distance between atom i and j. The parameters D_{OH} and α_{OH} entering the expression of the quartic potential describing the OH stretching motion were taken from ref 20. These parameters were shown to provide a reasonable description of the OH stretching frequencies when employed in quantum dynamical simulations of the infrared spectrum of liquid water.[20,37] In this regard, it is important to note that an accurate description of the OH infrared intensities also requires a proper description of the induced dipole interactions that cannot be accurately represented by any fixed charge models. The bending force constant K_{HOH} was kept fixed at the original value of the SPC/Fw model.[11] All other parameters that appear in eqs 2−4 were optimized using classical molecular dynamics (MD) simulations until an overall good agreement between the computed and the available experimental values was achieved for a relatively large set of water properties at 298.15 K, including radial distribution functions, density, enthalpy of vaporization, dielectric constant, diffusion coefficient, and orientational relaxation times. The final set of parameters that define the *a*SPC/Fw model is listed in Table 1.

All classical MD simulations were carried out with a development version of the AMBER suite of codes[38] and DL_POLY 2[39] for a system consisting of 256 water molecules in a periodic cubic

dx.doi.org/10.1021/jp208946p | *J. Phys. Chem. B* 2012, 116, 343–352

box. The short-range interactions were truncated at an atom−atom distance of 9.0 Å, while the electrostatic interactions were treated using the particle mesh Ewald method.[40] After 1 ns of equilibration, the structural and thermodynamic properties were calculated from a classical MD simulation of 5 ns performed in the isothermal−isobaric (NPT) ensemble with temperature and pressure maintained via Langevin dynamics and a Berendsen barostat,[40] respectively. The dielectric constant was instead calculated from a 4 ns simulation in the canonical (NVT) ensemble with the density held fixed at the corresponding calculated value. All the dynamical properties were obtained by averaging over 100 trajectories of 25 ps each carried out in the microcanonical (NVE) ensemble.

2.2. Anharmonic aMS-EVB3 Model. In the multistate empirical valence bond method the electronic wave function of a protonated system is represented by a linear combination of valence bond states that describe all possible molecular configurations of the hydronium ion (H_3O^+).[27−30] In practice, the valence bond configurations are generated by identifying first the "pivot hydronium" and then allowing the oxygen atoms of all water molecules located in the first three solvation shells of the pivot hydronium to also form hydronium ions. As in the MS-EVB3 model,[30,31] the solvation shells in the *a*MS-EVB3 model are determined using a geometric definition of the hydrogen bonds that involve the O---H distance (with a cutoff of 2.5 Å) between oxygen and hydrogen atoms of different molecules and the O−H---O angle (with a cutoff of 130°). In the parametrization of the new *a*MS-EVB3 model, the same functional form of the Hamiltonian is adopted as in the original MS-EVB3 model.[30,31] This implies that individual oxygen atoms are allowed to participate in more than one hydronium ion, which, as described in ref 30 is particularly important when the oxygen atoms of the water molecules are involved in two acceptor hydrogen bonds.

Following refs 30 and 31, the Hamiltonian matrix of the *a*MS-EVB3 model contains diagonal elements (H_{ii}), which describe both the intramolecular and intermolecular interactions of all molecules in each valence bond state, and off-diagonal elements (H_{ij}), which couple different states and effectively enable proton-hopping events from one water molecule to another. The diagonal terms take the form[30,31]

$$H_{ii} = V^{\text{intra}}(H_3O^+) + \sum_{k}^{N_{H_2O}} V_k^{\text{intra}}(H_2O) + \sum_{k}^{N_{H_2O}} V_k^{\text{inter}}(H_3O^+\text{-}H_2O) + \sum_{k<k'}^{N_{H_2O}} V_{kk'}^{\text{inter}}(H_2O\text{-}H_2O) \quad (5)$$

where $V^{\text{intra}}(H_3O^+)$ is the intramolecular potential of the hydronium ion expressed as

$$V^{\text{intra}}(H_3O^+) = \sum_{j}^{3} D_{OH}[1 - e^{-a_{OH}(r_{j,OH} - r_{OH}^{eq})}]^2 + \frac{1}{2}\sum_{j}^{3} k_\varphi(\varphi_{j,HOH} - \varphi_{HOH}^{eq})^2 \quad (6)$$

with $r_{j,OH}$ and $\varphi_{j,HOH}$ being the *j*th OH bond length and the *j*th HOH angle of the hydronium ion. The terms $V_k^{\text{intra}}(H_2O)$ and $V_{kk'}^{\text{inter}}(H_2O)$ are respectively the intra- and intermolecular potentials of the *a*SPC/Fw water model described in section 2.1. Finally, the term $V_k^{\text{inter}}(H_3O^+-H_2O)$ describes the interaction between the hydronium ion and the water molecules, and takes the form

$$V_k^{\text{inter}}(H_3O^+-H_2O) = 4\varepsilon_{OO_W}\left[\left(\frac{\sigma_{OO_W}}{R_{OO_W}}\right)^{12} - \left(\frac{\sigma_{OO_W}}{R_{OO_W}}\right)^{6}\right] + 4\varepsilon_{HO_W}\left[\left(\frac{\sigma_{HO_W}}{R_{HO_W}}\right)^{12} - \left(\frac{\sigma_{HO_W}}{R_{HO_W}}\right)^{6}\right] + \sum_{m}^{4}\sum_{n_k}^{3}\frac{q_m^{H_3O^+} q_{n_k}^{H_2O}}{R_{mn_k}} + V_{OO_k}^{\text{rep}} + V_{HO_k}^{\text{rep}} \quad (7)$$

This term includes the Lennard-Jones and Coulomb interactions between all pairs of nonbonded atoms as well as the two repulsive terms that were introduced in the MS-EVB3 model to correctly describe the interactions between the hydronium ion and the water molecules in the first solvation shell.[30] These latter terms are expressed as

$$V_{OO_k}^{\text{rep}} = Be^{-b(R_{OO_k} - d_{OO}^0)} \sum_{j}^{3} e^{-b' q_{H_jO_k}^2} \quad (8)$$

and

$$V_{HO_k}^{\text{rep}} = Ce^{-c(R_{HO_k} - d_{OH}^0)} \quad (9)$$

Following ref 30, the off-diagonal elements (H_{ij}) of the Hamiltonian matrix are defined as

$$H_{ij} = [V_{ij}^{(\text{const})} + V_{ij}^{(\text{ex})}]A(R_{OO}, q) \quad (10)$$

if the two valence bond states $|i\rangle$ and $|j\rangle$ share a common hydrogen atom, and $H_{ij} = 0$ otherwise. In eq 10, $V_{ij}^{(\text{const})}$ is a constant, while $V_{ij}^{(\text{ex})}$ describes the electrostatic interaction between the Zundel complex ($H_5O_2^+$) and the remaining $N_{H_2O} - 1$ water molecules and takes the form

$$V_{ij}^{(\text{ex})} = \sum_{m}^{7}\sum_{k}^{N_{H_2O}-1}\sum_{n_k}^{3}\frac{q_{n_k}^{H_2O} q_m^{ex}}{R_{mn_k}} \quad (11)$$

Here, q_m^{ex} and $q_{n_k}^{H_2O}$ are the exchange charges of the $H_5O_2^+$ complex and the atomic charges of the *k*th water molecule, respectively. The term $A(R_{OO},q)$ is instead a geometry-dependent scaling factor defined in ref 30 as

$$A(R_{OO}, q) = e^{-\gamma' q^2}[1 + Pe^{-k(R_{OO}-D_{OO})^2}] \times \left\{\frac{1}{2}\{1 - \tanh[\beta(R_{OO}-R_{OO}^0)]\} + P'e^{-\alpha(R_{OO}-r_{OO}^0)}\right\} \quad (12)$$

where R_{OO} is the distance between the two oxygen atoms of the $H_5O_2^+$ complex, and $q = (r_O + r_O^*)/(2) - r_{H^*}$ is the asymmetric stretch coordinate of the complex, with r_O and r_O^* being the position vectors of the two oxygen atoms and r_{H^*} being the corresponding vector of the central hydrogen atom. For a detailed description of all terms appearing in eqs 5−12, the interested reader is referred to refs 30 and 31.

The multidimensional optimization of the *a*MS-EVB3 parameters was performed with the genetic algorithm,[41,42] and the

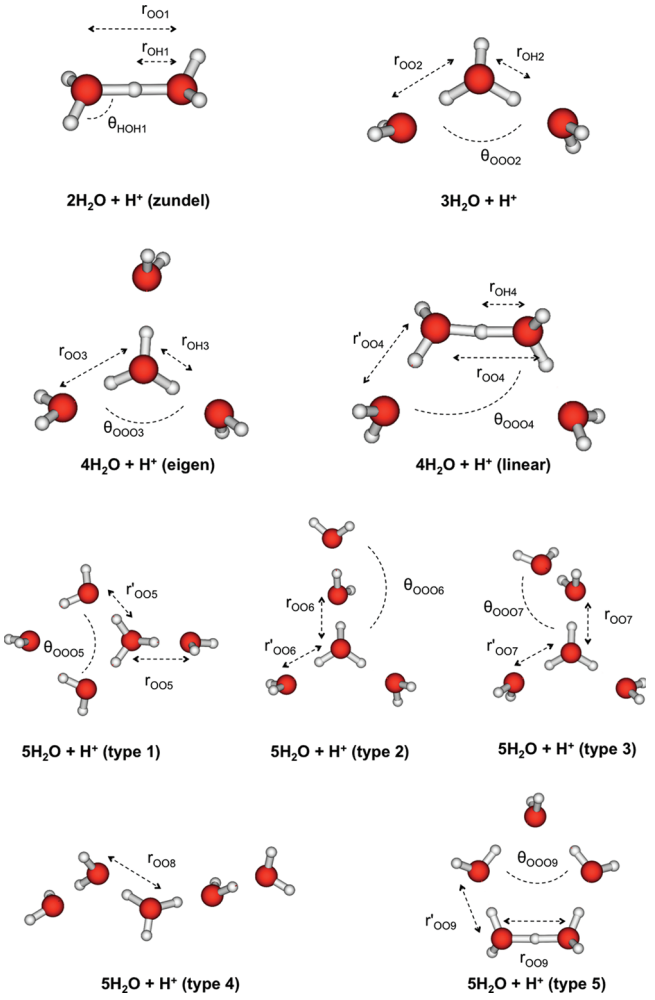

Figure 1. Geometries of protonated water dimer (Zundel ion), trimer, tetramers (Eigen ion and linear structure), and pentamers. The geometrical parameters indicated in the figure are listed in Table 4.

following target quantities were used: (1) ab initio geometries and binding energies of four different protonated water clusters shown in Figure 1, including the Zundel and Eigen structures as well as the cluster with 3 H_2O molecules and an excess proton; (2) ab initio potential energy surface (PES) associated with the proton shuttling between two water molecules in the Zundel configuration. The geometries of the water, hydronium ion, and protonated water clusters were optimized at the MP2/aug-cc-pVTZ level of theory. Single-point energy corrections at the CCSD(T)/aug-cc-pVTZ level of theory were then performed in order to obtain more accurate binding energies and proton shuttling PESs. All the ab initio calculations were performed using Gaussian 09.[43]

In the original MS-EVB3 model there are 33 independent parameters. Twenty-one parameters are associated with the diagonal elements, while the remaining 12 parameters are associated with the off-diagonal elements of the Hamiltonian matrix (eqs 5−12). Initially, 19 parameters were targeted during the parametrization of the new model. At this first stage, the parameters describing the smooth cutoff of the OO and HO repulsive terms in eqs 8 and 9 as well as those associated with the diagonal elements were kept fixed at the

Table 2. Parameters for the *a*MS-EVB3 Model

D_{OH}	(kcal/mol)	94.40010014	$r_{OO}^{sm,1a}$	(Å)	2.85
a_{OH}	($Å^{-1}$)	2.26724650	$r_{OO}^{sm,2b}$	(Å)	3.05
r_{OH}^{eq}	(Å)	1.0	$r_{OH}^{sm,1c}$	(Å)	2.50
k_{φ}	(kcal/mol/rad^2)	77.4868	$r_{OH}^{sm,2d}$	(Å)	3.00
φ_{HOH}^{eq}	(degree)	111.7269	V_{const}^{ij}	(kcal/mol)	−24.29325513
ε_{OOw}	(kcal/mol)	0.12074169	q_O^{ex}	(e)	−0.09290503
σ_{OOw}	(Å)	3.11941063	q_H^{ex}	(e)	0.03181478
ε_{HOw}	(kcal/mol)	0.00212056	$q_{H^*}^{ex}$	(e)	0.05855095
σ_{HOw}	(Å)	1.58086145	γ	($Å^{-2}$)	1.47116944
$q_O^{H_3O^+}$	(e)	−0.5	P		0.10342117
$q_H^{H_3O^+}$	(e)	0.5	k	($Å^{-2}$)	9.56531102
B	(kcal/mol)	11.28233555	D_{OO}	(Å)	3.00673285
b	($Å^{-1}$)	3.01657850	β	($Å^{-1}$)	7.05386835
b'	($Å^{-2}$)	2.40174399	R_{OO}^0	(Å)	3.04448208
d_{OO}^0	(Å)	2.40206347	P'	($Å^{-1}$)	7.58446749
C	(kcal/mol)	6.47644661	α	($Å^{-1}$)	7.19736309
c	($Å^{-1}$)	0.95362792	r_{OO}^0	(Å)	1.80176071
d_0^{OH}	(Å)	1.04900956			

[a] $r_{OO}^{sm,1}$: smooth cutoff starting distance for O−O repulsive term. [b] $r_{OO}^{sm,2}$: smooth cutoff ending distance for O−O repulsive term. [c] $r_{OH}^{sm,1}$: smooth cutoff starting distance for H−O repulsive term. [d] $r_{OH}^{sm,2}$: smooth cutoff ending distance for H−O repulsive term.

MS-EVB3 values. However, the first parametrization indicated that a new optimization of the intra- and intermolecular potential energy terms of the hydronium ion was necessary in order to obtain more accurate binding energies and PES properties of the protonated clusters. Therefore, six additional parameters were included in the parametrization, namely a_{OH} and D_{OH} describing the O−H stretch potential (eq 6) and the parameters associated with the Lennard-Jones potentials (eq 7). In conclusion, in the aMS-EVB3 model 25 parameters were reoptimized. The remaining parameters not included in the optimization procedure were kept fixed at the corresponding values of the original MS-EVB3 model. The final set of parameters for the *a*MS-EVB3 model is listed in Table 2.

The bulk properties of protonated water calculated with the *a*MS-EVB3 model were obtained using classical MD simulations for a system consisting of 256 water molecules and an excess proton in a periodic cubic box. Starting from an equilibrated configuration of 256 *a*SPC/Fw water molecules at T = 298.15 K and P = 1 atm, an excess proton was added to the simulation box and the combined system was further equilibrated for 1 ns at constant temperature and volume. The structural and thermodynamic properties were then calculated from a 1 ns long simulation in the NVT ensemble with the temperature controlled by a Nosé−Hoover thermostat with a relaxation time of 0.5 ps. The self-diffusion coefficient of the excess proton was instead calculated from an additional 5 ns simulation carried out in the NVE ensemble. An energy drift of 3.0 kcal mol^{-1} ns^{-1} was found in the NVE simulations, which is similar to the value (3.4 kcal mol^{-1} ns^{-1}) reported in ref 30 for the MS-EVB3 model. A modified version of DL_POLY2 was used for classical MD simulations.

3. RESULTS AND DISCUSSION

3.1. *a*SPC/Fw Model. Several structural, thermodynamic, and dynamical properties were computed with the new *a*SPC/Fw

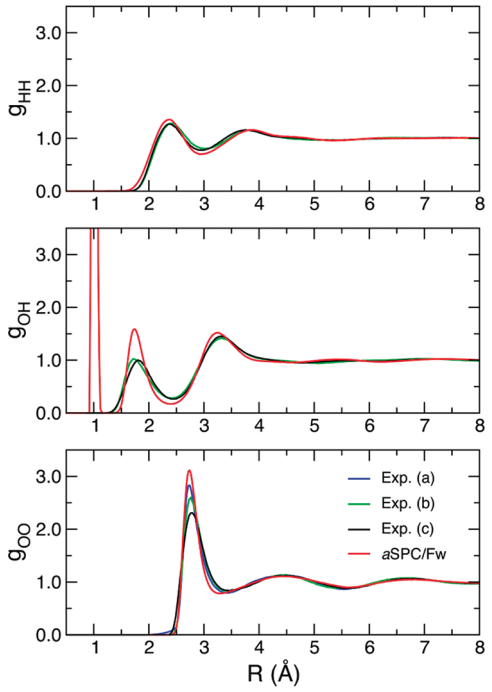

Figure 2. Radial distribution functions for oxygen−oxygen (bottom panel), oxygen−hydrogen (middle panel), and hydrogen−hydrogen (top panel) atom pairs computed with the *a*SPC/Fw water model. The experimental data for the set (a) are from ref 44 , set (b) are from ref 45, and set (c) are from ref 46.

model in order to assess its accuracy in reproducing the corresponding experimental values. First, the radial distribution functions (RDFs), calculated at T = 298.15 K, are compared in Figure 2 with the available data extracted from neutron and X-ray scattering measurements of the water structure factor.[44−46] It is worth mentioning that the precise determination of the local structure of liquid water is currently a matter of intense debate. The generally accepted picture of water as a liquid in which the molecules are on average 4-fold coordinated has been recently challenged by a different interpretation of X-ray absorption and emission spectra.[47−49] According to the new analysis, the arrangement of the water molecules within the first solvation shell is characterized by two distinct motifs that correspond respectively to tetrahedral and strongly distorted hydrogen-bonded configurations with a 1:2 ratio. The new proposed picture of the water structure is still highly controversial (e.g., see ref 50). The lack of consensus on a unique set of experimental data makes the direct comparison between simulation and experiment difficult. In an attempt to provide a general comparison, Figure 2 shows the RDFs calculated with the *a*SPC/Fw model along with the three experimentally derived sets that are most commonly employed in the literature. In all cases, the calculated RDFs qualitatively reproduce the main features of the corresponding experimental data, although they predict a slightly more structured liquid. This is particularly evident in the first peak of the OH RDF describing the correlation between oxygen and hydrogen atoms that are involved in hydrogen-bonded configurations. Due to the light mass of the hydrogen atoms, this peak is particularly sensitive to nuclear quantum effects that are neglected in this study. In this regard, it has been shown that, when nuclear quantization is explicitly taken into account in the molecular dynamics simulations, the agreement with the experimental data is significantly improved.[19] A similar reasoning can also be used to explain the differences between the calculated and experimental HH RDFs. Although the explicit inclusion of nuclear quantum effects is expected to improve the agreement with the experimental data for the OH and HH RDFs, the case of the OO RDF is somewhat different. As it is possible to see in the bottom panel of Figure 2, significant differences exist between the three sets of experimental data. Based on the calculations performed with the quantum qSPC/Fw model in ref 19, it may be expected that the inclusion of nuclear quantum effects will lower the height of the first peak located at ∼2.8 Å. However, the overall impact will be much smaller than that observed for the OH and HH RDFs due to the larger mass of the oxygen atoms.[19] Therefore, from a simple and qualitative analysis, it appears to be unlikely that, after inclusion of nuclear quantum effects, the OO RDF calculated with the new *a*SPC/Fw model could reproduce the experimentally derived data of ref 46. On the other hand, it may be expected that the quantum OO RDF can effectively reproduce the curves obtained in refs 44 and 45. If the present results are put in the context of other simulation studies, the RDFs calculated here with the *a*SPC/Fw model are similar to those obtained with other water force fields, including the empirical and nonpolarizable SPC/Fw,[11] TIP4P, E3B[14] models, and the ab initio-based and polarizable TTM3-F model.[15]

Table 3. Comparison between the Water Properties Calculated with the *a*SPC/Fw Model and the Corresponding Experimental Data[a]

property	*a*SPC/Fw	experiment	SPC/Fw
$\langle r_{OH}\rangle$ (Å)	1.0150 ± 0.0002	0.970[b]	1.0310 ± 10^{-6}
$\langle \theta_{HOH}\rangle$ (deg)	106.80 ± 0.05	106[c]	107.69 ± 0.33
$\langle \mu\rangle$ (D)	2.420 ± 0.005	2.9[d]	2.39 ± 0.19
ρ (g cm^{-3})	1.01 ± 0.01	0.997[e]	1.012 ± 0.016
ΔH_{vap} (kcal mol^{-1})	10.7 ± 0.1	10.52[f]	10.72 ± 0.12
C_p (kcal mol^{-1} K^{-1})	27.1 ± 0.1	17.99[g]	27.37
ε	88 ± 2	78.5[h]	79.63
α (10^{-4} K^{-1})	4.3 ± 0.1	2.0[i]	4.90
κ_T (10^{-5} atm^{-1})	4.6 ± 0.1	4.58[j]	4.50
D (Å^2 ps^{-1})	0.233 ± 0.001	0.229[k]	0.232 ± 0.05
τ_2 (ps)	2.7 ± 0.1	2.5[l]	1.86

[a] Also shown are the results obtained in ref 11 with the SPC/Fw model. All properties are described in the text. [b] From ref 54. [c] Derived from ref 54. [d] From ref 55. [e] From ref 56. [f] From ref 57. [g] From ref 58. [h] From ref 58. [i] From ref 59. [j] From ref 59. [k] From ref 60. [l] From ref 61.

Individual molecular properties were also calculated with the *a*SPC/Fw model. In particular, the average OH bond and HOH angle as well as the average molecular dipole moment are compared in Table 3 with the corresponding values obtained from simulations with the SPC/Fw model and from experiment. In all cases the present results are found to be in better agreement with the experimental data. The calculated dipole moment is still underestimated, which is common to all empirical force fields that, based on fixed partial atomic charges, are not able to correctly reproduce the molecular polarization arising in the bulk.

Besides the structural properties analyzed above, several thermodynamic quantities calculated with the *a*SPC/Fw model are also listed in Table 3. Similarly to the SPC/Fw model, the

density (ρ) of liquid water at T = 298.15 K is overestimated by ~2%. It must be noted, however, that the explicit inclusion of nuclear quantum effects has been shown to improve the agreement with the experimental value.[19] The enthalpy of vaporization was calculated according to the formula $\Delta H_{vap} \approx -\langle E\rangle + RT$, where $\langle E\rangle$ is the average potential energy and R is the gas constant. In order to make a direct comparison with the data reported in ref 11 for the SPC/Fw model, the corrections terms that are often applied to ΔH_{vap} were neglected. For a flexible, 3-point charge model these corrections amount to ~0.5 kcal mol^{-1}.[19] The static dielectric constant (ε) was instead computed according to the following expression

$$\varepsilon = 1 + \frac{4\pi}{3k_B VT}\left(\langle \mathbf{M}^2\rangle - \langle \mathbf{M}\rangle^2\right) \quad (13)$$

where $\mathbf{M}$ is the total dipole moment of the system, k_B is the Boltzmann constant, and V is the volume of the simulation box. The heat capacity at constant pressure was calculated as $C_P \approx (\Delta H)/(\Delta T)$, where H is the enthalpy of the system. For this purpose, two additional simulations of 1 ns each were carried out at T = 288.15 K and T = 308.15 K in the NPT ensemble. A correction factor that effectively takes into account for the quantum nature of the water vibrations is generally added to the classical C_P value. In the case of the *a*SPC/Fw model, this correction amounts to ~2 cal mol^{-1} and was determined numerically from path-integral molecular dynamics simulations. While both ΔH_{vap} and C_P calculated with the *a*SPC/Fw model are very similar to the corresponding values obtained with the SPC/Fw model, the dielectric constant is somewhat larger. This is likely due to the larger atomic partial charges (and, consequently, dipole moment) that are used in the present anharmonic model. Table 3 indicates that both the heat capacity and the dielectric constant calculated with the *a*SPC/Fw model are slightly larger than the corresponding experimental data. However, it has been shown that the inclusion of nuclear quantum effects generally leads to a decrease of the classical values, which results in a better agreement with the experimental data.[19]

Finally, the thermal expansion coefficient (α) and the isothermal compressibility (κ_T) for liquid water at T = 298.15 K were also calculated using the following expressions

$$\alpha = \frac{1}{V}\left(\frac{\partial V}{\partial T}\right)_P \approx -\left[\frac{\ln(\rho_2/\rho_1)}{T_2 - T_1}\right]_P \quad (14)$$

and

$$k_T = -\frac{1}{V}\left(\frac{\partial V}{\partial P}\right)_T \approx \left[\frac{\ln(\rho_2/\rho_1)}{P_2 - P_1}\right]_T \quad (15)$$

In order to compute α via eq 14, two additional NPT simulations of 1 ns each were carried out at T_1 = 288.15 K and T_2 = 308.15 K which were used to determine the corresponding densities. For the calculation of κ_T, two additional NVT simulations of 1 ns each were performed at T = 298.15 K to determine the corresponding pressure values that were used in eq 15. As shown in Table 3, both α and κ_T calculated with the *a*SPC/Fw model are in remarkably good agreement with the corresponding experimental results.

Several quantities associated with the dynamics of the water molecules in the bulk were also computed with the *a*SPC/Fw model. In particular, the diffusion coefficient was calculated through the velocity autocorrelation function according as

$$D = \frac{1}{3}\int \langle \mathbf{v}(0)\cdot\mathbf{v}(t)\rangle \, dt \quad (16)$$

where $\mathbf{v}$ is the center-of-mass velocity of a water molecule. The relaxation time (τ_2) associated with the reorientation of the water molecules within the hydrogen-bond network was instead obtained from the exponential fit of the long-time decay of the following orientational correlation function

$$C_2(t) = \langle P_2[\mathbf{e}_{OH}(0)\cdot\mathbf{e}_{OH}(t)]\rangle \quad (17)$$

Here, P_2 is the second Legendre polynomial and $\mathbf{e}$ is a unit vector along the OH bonds of a water molecule. As shown in Table 3, both D and τ_2 calculated with the *a*SPC/Fw model are in good agreement with the corresponding experimental data. Furthermore, while the diffusion coefficient is similar to the value obtained with the SPC/Fw model, the new *a*SPC/Fw model clearly provides a more accurate description of the water orientational dynamics.

The comparison reported in Table 3 thus indicates that the new *a*SPC/Fw model provides an overall better description of bulk water relative to the SPC/Fw model. This is particularly evident from the analysis of the properties that are associated to individual molecules (such as the equilibrium geometry and dipole moment) as well as to the dynamics of the hydrogen-bond network (such as the C_2 orientational correlation function). In the next section, it will be shown that this improved description of the water properties lead to a significantly more accurate description of the mobility of excess protons in water.

3.2. *a*MS-EVB3 Model. The optimized geometries of the protonated water clusters calculated with the *a*MS-EVB3, MS-EVB3, and MP2/aug-cc-pVTZ methods are listed in Table 4, which also includes the data for the protonated clusters containing 5 H_2O molecules (Figure 1) that were not part of the training set used to parametrized the new *a*MS-EVB3 model. In all cases, the values obtained with the *a*MS-EVB3 model for the structural properties are in good agreement with the corresponding ab initio data, with the largest bond and angle differences being 0.04 Å for the O−H bond of the Eigen ion ($H_9O_4^+$) and 6.3° for the O---O---O angle of the protonated water trimer, respectively. All ab initio binding energies of the protonated water clusters, including those with 5 H_2O molecules that were not used in the parametrization, are accurately reproduced by the *a*MS-EVB3 model (Table 5). Tables 4 and 5 also indicate that overall both the structural properties and energetics calculated with the new *a*MS-EVB3 model are in better agreement with the corresponding ab initio values than those obtained with the original MS-EVB3 model.

Four curves describing radial cuts of the PES associated with the shuttling motion of the excess proton in the Zundel configuration were calculated for O---O separations corresponding to 2.2, 2.4, 2.6, and 2.8 Å, respectively. Following ref 30, the coordinate q describing the proton shuttling motion was defined as the distance of the central hydrogen atom from its equilibrium position while keeping the O---O distance fixed. For each value of the O---O distance, the scan along q was carried out at the CCSD(T)/aug-cc-pVTZ level of theory with all the internal coordinates being kept fixed at the optimized values obtained with MP2/aug-cc-pVTZ. All four curves were included in the parametrization of the *a*MS-EVB3 model. Figure 3 shows a comparison between the ab initio data and the results obtained with the *a*MS-EVB3 model. In all cases, an excellent agreement is

Table 4. Geometries of Protonated Water Clusters[a]

	int coord[b]	*a*MS-EVB3	MS-EVB3[c]	MP2/aug-cc-pVTZ
$2H_2O + H^+$ (Zundel)	r_{OO1}	2.37	2.39	2.40
	r_{OH1}	1.19	1.20	1.20
	θ_{HOH1}	117.6	117.3	115.8
$3H_2O + H^+$	r_{OO2}	2.49	2.50	2.49
	r_{OH2}	1.07	1.07	1.04
	θ_{OOO2}	110.8	110.6	117.1
$4H_2O + H^+$ (Eigen)	r_{OO3}	2.53	2.55	2.55
	r_{OH3}	1.05	1.07	1.01
	θ_{OOO3}	108.4	108.4	114.1
$4H_2O + H^+$ (linear)	r_{OO4}	2.37	2.37	2.39
	r'_{OO4}	2.59	2.59	2.59
	r_{OH4}	1.18	1.19	1.20
	θ_{OOO4}	115.7	114.7	119.1
$5H_2O + H^+$ (type 1)	r_{OO5}	2.54	2.55	2.57
	r'_{OO5}	2.54	2.51	2.54
	θ_{OOO5}	78.1	75.6	79.0
$5H_2O + H^+$ (type 2)	r_{OO6}	2.44	2.46	2.47
	r'_{OO6}	2.55	2.56	2.59
	θ_{OOO6}	120.2	120.2	117.4
$5H_2O + H^+$ (type 3)	r_{OO7}	2.45	2.46	2.47
	r'_{OO7}	2.56	2.57	2.59
	θ_{OOO7}	125.2	125.0	121.9
$5H_2O + H^+$ (type 4)	r_{OO8}	2.49	2.48	2.46
$5H_2O + H^+$ (type 5)	r_{OO9}	2.37	2.37	2.39
	r'_{OO9}	2.57	2.58	2.57
	θ_{OOO9}	85.7	85.0	91.3

[a] Units are in angstroms for distances and degree for angles. [b] All coordinates are defined Figure 1. [c] From ref 30. The MS-EVB3 geometries for the $5H_2O + H^+$ clusters were directly computed using the force field parameters reported in refs 30 and 37.

Table 5. Comparison of Binding Energies of Protonated Water Clusters[a]

	*a*MS-EVB3	MS-EVB3[b]	CCSD(T)//MP2/aug-cc-pVTZ
$2H_2O + H^+$ (Zundel)	−32.83	−33.05	−33.47
$3H_2O + H^+$	−56.64	−57.18	−57.65
$4H_2O + H^+$ (Eigen)	−79.05	−79.70	−77.55
$4H_2O + H^+$ (linear)	−73.89	−73.90	−73.68
$5H_2O + H^+$ (type 1)	−91.93	−93.64	−92.21
$5H_2O + H^+$ (type 2)	−93.52	−93.85	−91.15
$5H_2O + H^+$ (type 3)	−93.56	−93.96	−91.17
$5H_2O + H^+$ (type 4)	−87.67	−87.67	−87.63
$5H_2O + H^+$ (type 5)	−89.14	−89.41	−88.61

[a] Units are in kcal mol^{-1}. [b] From ref 30.

achieved, with the largest difference between the ab initio and *a*MS-EVB3 curves being ~1 kcal/mol for an O---O separation of 2.6 Å.

In order to analyze the structural properties of protonated water, several RDFs were calculated which are compared in Figure 4 with the corresponding experimental data of ref 51. Both

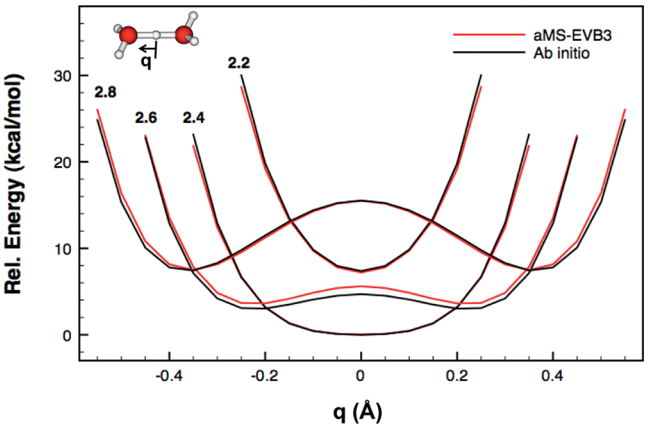

Figure 3. PES curves for the proton shuttling in the Zundel ion with O---O distances of 2.2, 2.4, 2.6, and 2.8 Å. The proton shuttling coordinate, *q*, is defined as the difference in the distance of the central hydrogen from its position at the center. See the section 3.2 for details.

the O−O* RDF describing the spatial correlation between the oxygen atoms (O) of the water molecules and the oxygen atom (O*) of the pivot hydronium ion, and the O−H* RDF describing the spatial correlation between the oxygen atoms of the water molecules and the hydrogen atoms (H*) of the pivot hydronium ion calculated with the *a*MS-EVB3 model are similar to the corresponding RDFs obtained with the original MS-EVB3 model.[30] This is not completely unexpected since both models provide a similar description of the protonated water clusters as described above.

A significant improvement is instead provided by the new *a*MS-EVB3 model in the description of the proton mobility in bulk water. Following ref 30, the self-diffusion coefficient of the excess proton was calculated from the mean-square displacement (MSD) of the center of excess charge (CEC) defined as

$$\mathbf{r}_{CEC} = \sum_{i}^{N} c_i^2 \mathbf{r}^i_{COC} \tag{18}$$

where $\mathbf{r}^i_{COC}$ is the center of charge of the hydronium ion in the *i*th EVB state. The Einstein relation, defined in eq 19, was then used to calculate the self-diffusion coefficient of the center of excess charge (D_{CEC})

$$D_{CEC} = \lim_{t \to \infty} \frac{\langle |\mathbf{r}_{CEC}(t) - \mathbf{r}_{CEC}(0)|^2 \rangle}{6t} \tag{19}$$

The self-diffusion coefficient calculated with the *a*MS-EVB3 model is D_{CEC} = 0.410 ± 0.002 $Å^2$/ps (the error is from 95% confidence bounds after the linear least-squares fit), which is ~40% larger than the corresponding value obtained with the original MS-EVB3 model as shown in Figure 5. This difference can be qualitatively explained by calculating the free energy for proton transfer expressed as $\Delta F = -kT \ln(c_1^2 - c_2^2)$, where c_1 and c_2 are the largest and second largest amplitudes in the MS-EVB expansion of the total wave function. Although it has been shown that the actual reaction coordinate describing proton transfer in water involves the collective rearrangement of the hydrogen-bond network, the free energy calculated within the MS-EVB framework as a function of $c_1^2 - c_2^2$ still provides useful insights into the associated energetics since the pivot state has to change identity when $c_1^2 - c_2^2 = 0$, which effectively corresponds

dx.doi.org/10.1021/jp208946p | *J. Phys. Chem. B* 2012, 116, 343–352

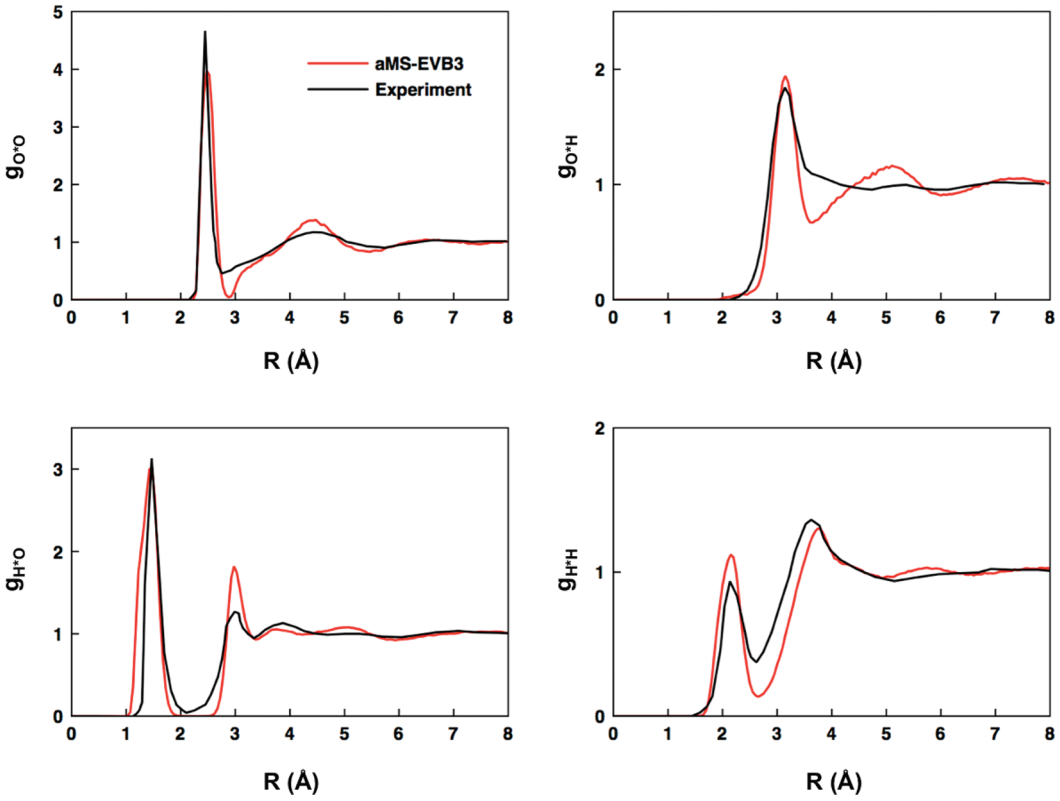

Figure 4. RDF curves of bulk water with an excess proton. (a) Top left panel: RDF describing the spatial correlation between the oxygen atom of the pivot hydronium ion (O*) and the water oxygen atoms (O). (b) Top right panel: RDF describing the spatial correlation between the oxygen atom of the pivot hydronium ion (O*) and the water hydrogen atoms (H). (c) Bottom left panel: RDF describing the spatial correlation between the hydrogen atoms of the pivot hydronium ion (H*) and the water oxygen atoms (O). (d) Bottom right panel: RDF describing the spatial correlation between the hydrogen atoms in the pivot hydronium ion (H*) and the water hydrogen atoms (H). The experimental data are from ref 51.

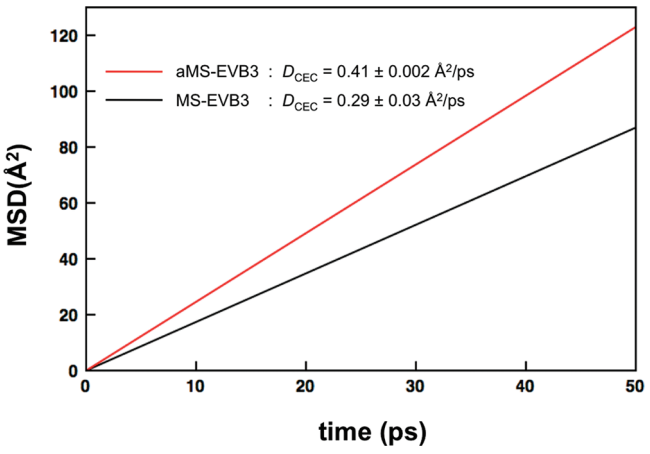

Figure 5. Mean-square displacement (MSD) of the excess proton center of the excess charge as a function of time. The data for the MS-EVB3 model are from ref 30.

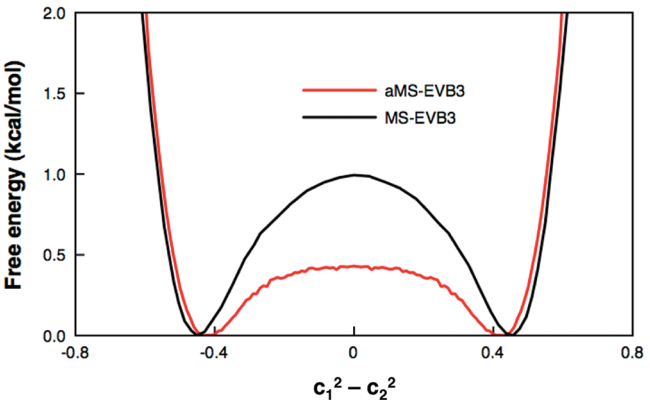

Figure 6. Comparison of the *a*MS-EVB3 (red) and MS-EVB3 (black) free energy profiles for the proton-transfer reaction calculated as a function of the difference between the two largest MS-EVB amplitudes, $c_1^2 - c_2^2$. The MS-EVB3 results are from ref 30.

to a proton-hopping event. As shown in Figure 6, the free-energy barrier calculated with the present *a*MS-EVB3 model is appreciably lower than that obtained in ref 30 with the original MS-EVB3 model, which correlates well with the difference in the corresponding self-diffusion coefficients of the center of excess charge.

The present results thus suggest that a description of the O−H stretching motion of the water molecules in terms of a more physically realistic anharmonic potential is an important component for a more quantitative molecular-level representation of the dynamical properties of the excess proton in aqueous environments. However, although the significant improvement over the original MS-EVB3 model, the value of the self-diffusion coefficient calculated with the *a*MS-EVB3 model is still somewhat smaller than the corresponding experimental value of 0.94 ± 0.01 Å^2/ps. One possible reason for this difference can be related

dx.doi.org/10.1021/jp208946p |*J. Phys. Chem. B* 2012, 116, 343–352

to the fact that the present *a*MS-EVB3 model has been specifically developed for classical simulations, which implies that nuclear quantum effects are not explicitly taken into account. As shown in ref 30, the explicit inclusion of nuclear quantum effects in the qMS-EVB3 model, in which the water interactions are described in terms of the quantum qSPC/Fw model, results in a ∼70% increase of the self-diffusion coefficient. A similar scaling factor can be expected for the quantum version of the present aMS-EVB3 model in which the water interactions will be represented by the quantum analog of the aSPC/Fw model described here. Within this hypothesis, if such a factor is applied to the present D_{CEC} value, the scaled result would be found within ∼25% of the experimental value. In this regard, it can be expected that nuclear quantum effects will be more pronounced in the case of the *a*MS-EVB3 model due to the anharmonicity of the underlying water model. Work along these lines is currently underway in our group. Another possible reason for the difference between the value calculated with the *a*MS-EVB3 model and the experimental estimate can be related to the fact that polarization effects are only partially taken into account within the *a*MS-EVB3 representation of the system Hamiltonian. A quantitative analysis of the impacts of both polarization and nuclear quantum effects on the mobility of protons in aqueous environments clearly deserves further investigation in future developments of the MS-EVB models.

4. CONCLUSIONS

In this study, a refined MS-EVB model (*a*MS-EVB3) has been developed in order to improve the description of the proton mobility in aqueous environments. The new *a*MS-EVB3 model is built upon an anharmonic water force field (*a*SPC/Fw) in which the OH stretching motion is described by a quartic approximation to a Morse potential. Through an extended analysis of several structural, thermodynamic, and dynamical properties, it is shown that the anharmonic *a*SPC/Fw model provides an improved description of the behavior of water at ambient conditions relative to its harmonic counterpart. In particular, single-molecule structural properties such as the equilibrium bond distance and angle are in better agreement with the corresponding experimental values. Importantly, the new model also provides a more accurate representation of the orientational dynamics of water molecules in the liquid phase, which is directly connected with the rearrangements of the hydrogen-bond network.

The anharmonic *a*SPC/Fw water force field is used as a basis for developing an improved version of the multistate empirical valence bond model, the *a*MS-EVB3 model. The latter is shown to provide an accurate description of the solvation structure of an excess proton in bulk water, which is in good agreement with the available experimental data as well as with the results obtained with the previous (harmonic) MS-EVB3 model. Importantly, the new *a*MS-EVB3 model predicts a significantly larger (∼40%) proton diffusion coefficient compared to MS-EVB3, which improves the agreement with the experimental estimate of proton mobility in water. This indicates that a more physically correct description of the water properties plays an important role in the description of the hopping events associated with the motion of excess protons in aqueous environments. Although the present result represents an appreciable improvement over previous calculations within the nonpolarizable MS-EVB framework, a noticeable difference still exists between the calculated value and the experimental estimate. Possible reasons for this difference can be associated with nuclear quantum effects and explicit polarization effects which are neglected in the *a*MS-EVB3. In this regard, it has been shown that the inclusion of nuclear quantum effects into a specifically designed quantum version of the MS-EVB3 model leads to a ∼70% increase of the proton diffusion coefficients relative to the classical counterpart. Since nuclear quantum effects are more pronounced for anharmonic potentials, a similar or even larger factor may be expected from quantum simulations with an appropriate quantum version of the *a*MS-EVB3 model. A more detailed analysis of the role played by both polarization and nuclear quantum effects on the mobility of protons in aqueous environments clearly deserves further investigation in future developments of the MS-EVB models. In this regard, the use of more sophisticated water models derived from high-level ab initio calculations[52,53] could lead to an overall more accurate description of proton solvation and transport in the condensed phase.

AUTHOR INFORMATION

Corresponding Author

*E-mail: fpaesani@ucsd.edu.

Author Contributions

†These authors contributed equally.

ACKNOWLEDGMENT

This research was supported by the National Science Foundation through grant CHE-1111364. We are grateful to the National Science Foundation for a generous allocation of computing time on Teragrid resources as well as to the San Diego Supercomputer Center for a computing time allocation on the Triton Computing Cluster through the TRO program.

REFERENCES

(1) Maréchal, Y. *The hydrogen bond and the water molecule: The physics and chemistry of water, aqueous and bio-media*; Elsevier: Amsterdam, 2006.

(2) Ball, P. *Life's matrix: A biography of water*; University of California Press: Berkeley, CA, 2001.

(3) Swanson, J. M. J.; Maupin, C. M.; Chen, H.; Petersen, M. K.; Xu, J.; Wu, Y.; Voth, G. A. *J. Phys. Chem. B* **2007**, *111*, 4300–4314.

(4) Marx, D. *ChemPhysChem* **2006**, *7*, 1848–1870.

(5) Molinero, V.; Moore, E. B. *J. Phys. Chem. B* **2009**, *113*, 4008–4016.

(6) Izvekov, S.; Parrinello, M.; Burnham, C. J.; Voth, G. A. *J. Chem. Phys.* **2004**, *120*, 10896–10913.

(7) Abascal, J. L. F.; Vega, C. *J. Chem. Phys.* **2005**, *123*, 234505.

(8) Berendsen, H. J. C.; Grigera, J. R.; Straatsma, T. P. *J. Phys. Chem.* **1987**, *91*, 6269.

(9) Jorgensen, W. L.; Chandrasekhar, J.; Madura, J. D.; Impey, R. W.; Klein, M. L. J. *Chem. Phys.* **1983**, *79*, 926–935.

(10) Horn, H. W.; Swope, W. C.; Pitera, J. W.; Madura, J. D.; Dick, T. J.; Hura, G. L.; Head-Gordon, T. *J. Chem. Phys.* **2004**, *120*, 9665–9678.

(11) Wu, Y. J.; Tepper, H. L.; Voth, G. A. *J. Chem. Phys.* **2006**, *124*, 024503.

(12) Bukowski, R.; Szalewicz, K.; Groenenboom, G. C.; van der Avoird, A. *J. Chem. Phys.* **2008**, *128*, 094314.

(13) Wang, Y.; Bowman, J. M. *Chem. Phys. Lett.* **2010**, *491*, 1–10.

(14) Tainter, C. J.; Pieniazek, P. A.; Lin, Y. S.; Skinner, J. L. *J. Chem. Phys.* **2011**, *134*, 184501.

(15) Fanourgakis, G. S.; Xantheas, S. S. *J. Chem. Phys.* **2008**, *128*, 074506.

(16) Burnham, C. J.; Anick, D. J.; Mankoo, P. K.; Reiter, G. F. *J. Chem. Phys.* **2008**, *128*, 154519.
(17) Mankoo, P. K.; Keyes, T. *J. Chem. Phys.* **2008**, *129*, 034504–034509.
(18) Lobaugh, J.; Voth, G. A. *J. Chem. Phys.* **1997**, *106*, 2400–2410.
(19) Paesani, F.; Zhang, W.; Case, D. A.; Cheatham, T. E.; Voth, G. A. *J. Chem. Phys.* **2006**, *125*, 184507.
(20) Habershon, S.; Markland, T. E.; Manolopoulos, D. E. *J. Chem. Phys.* **2009**, *131*, 024501.
(21) de Grotthuss, C. J. T. *Ann. Chim.* **1806**, *58*, 54.
(22) Swanson, J. M. J.; Simons, J. *J. Chem. Phys. B* **2009**, *113*, 5149–5161.
(23) Lin, I. C.; Seitsonen, A. P.; Coutinho-Neto, M. D.; Tavernelli, I.; Rothlisberger, U. *J. Phys. Chem. B* **2009**, *113*, 1127–1131.
(24) Murdachaew, G.; Mundy, C. J.; Schenter, G. K. *J. Chem. Phys.* **2010**, *132*, 164102.
(25) Yoo, S.; Xantheas, S. S. *J. Chem. Phys.* **2011**, *134*, 121105.
(26) Wang, J.; Roman-Perez, G.; Soler, J. M.; Artacho, E.; Fernandez-Serra, M. V. *J. Chem. Phys.* **2011**, *134*, 024516.
(27) Schmitt, U. W.; Voth, G. A. *J. Phys. Chem. B* **1998**, *102*, 5547–5551.
(28) Schmitt, U. W.; Voth, G. A. *J. Chem. Phys.* **1999**, *111*, 9361–9381.
(29) Day, T. J. F.; Soudackov, A. V.; Cuma, M.; Schmitt, U. W.; Voth, G. A. *J. Chem. Phys.* **2002**, *117*, 5839–5849.
(30) Wu, Y.; Chen, H.; Wang, F.; Paesani, F.; Voth, G. A. *J. Phys. Chem. B* **2008**, *112*, 467–482.
(31) Wu, Y.; Chen, H.; Wang, F.; Paesani, F.; Voth, G. A. *J. Phys. Chem. B* **2008**, *112*, 7146–7146.
(32) Vuilleumier, R.; Borgis, D. *J. Phys. Chem. B* **1998**, *102*, 4261.
(33) Vuilleumier, R.; Borgis, D. *J. Chem. Phys.* **1999**, *111*, 4251.
(34) Warshel, A. *Computer Modeling of Chemical Reactions in Enzymes and Solutions*; Wiley-Interscience: New York, 1991.
(35) Markovitch, O.; Chen, H.; Izvekov, S.; Paesani, F.; Voth, G. A.; Agmon, N. *J. Phys. Chem. B* **2008**, *112*, 9456–9466.
(36) Brancato, G.; Tuckerman, M. E. *J. Chem. Phys.* **2005**, *122*, 224507.
(37) Paesani, F.; Voth, G. A. *J. Chem. Phys.* **2010**, *132*, 014105.
(38) Case, D. A.; Darden, T. A.; Cheatham, T. E., III; Simmerling, C. L.; Wang, J.; Duke, R. E.; Luo, R.; Crowley, M.; Walker, R. C.; Zhang, W.; Merz, K. M.; Roberts, B.; Wang, B.; Hayik, S.; Roitberg, A.; Seabra, G.; Kolossváry, I.; Wong, K. F.; Paesani, F.; Vaníček, J.; Wu, X.; Brozell, S. R.; Steinbrecher, T.; Gohlke, H.; Cai, Q.; Ye, X.; Wang, J.; Hsieh, M.-J.; Cui, G.; Roe, D. R.; Mathews, D. H.; Seetin, M. G.; Sagui, C.; Babin, V.; Luchko, T.; Gusarov, S.; Kovalenko, A.; Kollman, P. A. *AMBER 11*, 11th ed.; University of California—San Francisco: San Francisco, 2010.
(39) Smith, W.; Forester, T. *J. Mol. Graphics* **1996**, *14*, 136.
(40) Frenkel, D.; Smit, B. *Understanding molecular simulation: From algorithms to applications*; Academic Press: New York, 2001.
(41) Goldberg, D. E. *Genetic Algorithms in Search, Optimization and Machine Learning*, 1st ed.; Addison-Wesley Longman Publishing Co., Inc.: Boston, MA, 1989.
(42) Carroll, D. L. FORTRAN Genetic Algorithm (GA) Driver.
(43) Frisch, M. J.; Trucks, G. W.; Schlegel, H. B.; Scuseria, G. E.; Robb, M. A.; Cheeseman, J. R.; Scalmani, G.; Barone, V.; Mennucci, B.; Petersson, G. A.; Nakatsuji, H.; Caricato, M.; Li, X.; Hratchian, H. P.; Izmaylov, A. F.; Bloino, J.; Zheng, G.; Sonnenberg, J. L.; Hada, M.; Ehara, M.; Toyota, K.; Fukuda, R.; Hasegawa, J.; Ishida, M.; Nakajima, T.; Honda, Y.; Kitao, O.; Nakai, H.; Vreven, T.; Montgomery, J. A., Jr. ; Peralta, J. E.; Ogliaro, F.; Bearpark, M.; Heyd, J. J.; Brothers, E.; Kudin, K. N.; Staroverov, V. N.; Kobayashi, R.; Normand, J.; Raghavachari, K.; Rendell, A.; Burant, J. C.; Iyengar, S. S.; Tomasi, J.; Cossi, M.; Rega, N.; Millam, J. M.; Klene, M.; Knox, J. E.; Cross, J. B.; Bakken, V.; Adamo, C.; Jaramillo, J.; Gomperts, R.; Stratmann, R. E.; Yazyev, O.; Austin, A. J.; Cammi, R.; Pomelli, C.; Ochterski, J. W.; Martin, R. L.; Morokuma, K.; Zakrzewski, V. G.; Voth, G. A.; Salvador, P.; Dannenberg, J. J.; Dapprich, S.; Daniels, A. D.; Farkas, Ö.; Foresman, J. B.; Ortiz, J. V.; Cioslowski, J.; Fox, D. J. *Gaussian 09, Rev. A.1*; Gaussian, Inc.: Wallingford, CT, 2009.
(44) Hura, G.; Russo, D.; Glaeser, R. M.; Head-Gordon, T.; Krack, M.; Parrinello, M. *Phys. Chem. Chem. Phys.* **2003**, *5*, 1981–1991.
(45) Soper, A. K.; Benmore, C. J. *Phys. Rev. Lett.* **2008**, *101*, 065502.
(46) Wikfeldt, K. T.; Leetmaa, M.; Ljungberg, M. P.; Nilsson, A.; Pettersson, L. G. M. *J. Phys. Chem. B* **2009**, *113*, 6246–6255.
(47) Wernet, P.; Nordlund, D.; Bergmann, U.; Cavalleri, M.; Odelius, M.; Ogasawara, H.; Näslund, L. Å.; Hirsh, T. K.; Ojamäe, L.; Glatzel, P.; Pettersson, L. G. M.; Nilsson, A. *Science* **2004**, *304*, 995–999.
(48) Tokushima, T.; Harada, Y.; Takahashi, O.; Senba, Y.; Ohashi, H.; Pettersson, L. G. M.; Nilsson, A.; Shin, S. *Chem. Phys. Lett.* **2008**, *460*, 387–400.
(49) Huang, C.; Wikfeldt, K. T.; Tokushima, T.; Nordlund, D.; Harada, Y.; Bergmann, U.; Niebuhr, M.; Weiss, T. M.; Horikawa, Y.; Leetmaa, M.; Ljungberg, M. P.; Takahashi, O.; Lenz, A.; Ojamae, L.; Lyubartsev, A. P.; Shin, S.; Pettersson, L. G. M.; Nilsson, A. *Proc. Natl. Acad. Sci. U.S.A.* **2009**, *106*, 15214–15218.
(50) Clark, G. N. I.; Cappa, C. D.; Smith, J. D.; Saykally, R. J.; Head-Gordon, T. *Mol. Phys.* **2010**, *108*, 1415–1433.
(51) Botti, A.; Bruni, F.; Imberti, S.; Ricci, M. A.; Soper, A. K. *J. Chem. Phys.* **2004**, *121*, 7840–7848.
(52) Cencek, W.; Szalewicz, K.; Leforestier, C.; van Harrevelt, R.; van der Avoird, A. *Phys. Chem. Chem. Phys.* **2008**, *10*, 4716–4731.
(53) Wang, Y.; Shepler, B. C.; Braams, B. J.; Bowman, J. M. *J. Chem. Phys.* **2009**, *131*, 054511–054518.
(54) Ichikawa, K.; Kameda, Y.; Yamaguchi, T.; Wakita, H.; Misawa, M. *Mol. Phys.* **1991**, *73*, 79–86.
(55) Badyal, Y. S.; Saboungi, M. L.; Price, D. L.; Shastri, S. D.; Haeffner, D. R.; Soper, A. K. *J. Chem. Phys.* **2000**, *112*, 9206–9208.
(56) Kell, G. S. *J. Chem. Eng. Data* **1967**, *12*, 66–69.
(57) Wagner, W.; Pruss, A. *J. Phys. Chem. Ref. Data* **2002**, *31*, 387–535.
(58) *Handbook of Chemistry and Physics*; Haynes, W. M., Ed.; CRC Press: Boca Raton, FL, 2011.
(59) *Water: A comprehensive treatise*; Franks, F., Ed.; Plenum: New York, 1972.
(60) Krynicki, K.; Green, C. D.; Sawyer, D. W. *Faraday Discuss.* **1978**, *66*, 199–208.
(61) Bakker, H. J.; Rezus, Y. L. A.; Timmer, R. L. A. *J. Phys. Chem. A* **2008**, *112*, 11523–11534.